Catalytic Role of Intercalated Pt Complex in Thermal Decomposition of Nitrate-Type Hydrotalcite to Porous Structure

Shin Hamada, Keita Ikeue, and Masato Machida*

Department of Applied Chemistry and Biochemistry, Faculty of Engineering, Kumamoto University, Kumamoto 860-8555, Japan

Received May 21, 2005. Revised Manuscript Received July 15, 2005

Thermal decomposition of $PtCl_6$-exchanged hydrotalcite-like $Mg_{0.74}Al_{0.26}(OH)_2(NO_3)_{0.26}\cdot 0.36H_2O$ (Pt−HT) in a stream of H_2 has been investigated to demonstrate the catalytic role of intercalated Pt on the transformation to porous structures. Platinum species in the interlayer promoted the reaction between H_2 and interlayer nitrate (NO_3^-) to yield N_2 so as to give rise to a large surface area (≥ 200 m^2 g^{-1}) solid at as low as ca. 200 °C, compared to 400 °C required for the pristine HT. The XAFS analysis of the $PtCl_6$-exchanged HT gave evidence that part of chloride (Cl^-) ligands bound to Pt was replaced by NO_3^- during an exchange process. Since molecular hydrogen is activated by Pt, the reaction of nitrate ligand with hydrogen to form N_2/H_2O should generate a vacant site, which is successively occupied by NO_3^- ions lying in the interlayer. Such coordination/catalytic reduction cycles would accelerate the removal of NO_3^- surrounding Pt in the interlayer before dehydroxylation of brucite layers. This is in contrast to the pristine HT, where the release of NO_3^- as NO and dehydroxylation occurred simultaneously at ≥400 °C. Consequently, N_2 adsorption/desorption isotherms showed the two-dimensional pore structure of Pt−HT in contrast to the three-dimensional pores of the pristine HT after thermal decomposition.

Introduction

Hydrotalcite-like double-layered hydroxides can accommodate a large number of di- and trivalent cations in $M(OH)_6$ octahedra, which are linked by sharing their edge to form a brucite-type layered structure.[1−4] Positive charges of the layer originating from the trivalent cation are compensated by interlayer anions such as NO_3^-, CO_3^{2-}, SO_4^{2-}, etc., so these compounds become anionic exchangers. The materials of this family are very useful as catalyst precursors because a large surface area porous structure can easily be obtained by thermal decomposition regardless of the morphology and crystallinity of starting hydrotalcites.[1,5−7] When an Mg−Al hydrotalcite is thermally decomposed, a product consisting of noncrystalline MgO-like phase possesses a large surface area of ≥ 100 m^2 g^{-1}, compared to less than 5 m^2 g^{-1} before heating. Such a significant increase of surface area is closely related to the decomposition mechanism.

The thermal decomposition of the Mg−Al hydrotalcite takes place in a two-step process consisting of a preliminary loss of interlayer water molecules at 50−150 °C and the collapse of layered hydroxide at higher temperatures.[8] Recently, Bellotto et al.[9] reported that the structural evolution during the collapse can be divided into two different stages, i.e., the elimination of interlayer anions and dehydroxylation of brucite layers. After these two stages, the layer structure is converted into a three-dimensional texture having a substantial structural strain, which causes the increase of surface area. The depletion of anions and the dehydroxylation are linked, the extent of this depending upon the type as well as the content of interlayer anions. For instance, the escape of CO_2 from Mg−Al−CO_3 generally overlaps with the dehydroxylation process.[10,11] Zeng and his co-worker[12] reported that the decomposition pathway of Mg−Al−NO_3 is dependent on the content of nitrate. At a low nitrate content, the dehydroxylation of brucite layers takes place at 300−380 °C prior to the decomposition of NO_3^- to evolve NO_2/O_2 at 360−540 °C. By contrast, these two processes in a high nitrate content phase are overlapped because of the shift of dehydroxylation toward higher temperatures. This is indicative of improved thermal stability of brucite layers as a result of interaction between the hydroxyl groups and nitrates in the interlayer.

The thermal behavior of Mg−Al−NO_3 is also influenced by metal species introduced by anion exchange. We have recently reported that only a small amount of $PtCl_6^{2-}$ exchanged into $Mg_{1-x}Al_x(OH)_2(NO_3)_x$ ($2Pt/Al = 0.03$) has a noticeable effect on the thermal decomposition in a stream

* To whom correspondence should be addressed. Fax/Tel: +81-96-342-3651. E-mail: machida@chem.kumamoto-u.ac.jp.

(1) Cavani, F.; Trifiro, F.; Vaccari, A. *Catal. Today* **1991**, *11*, 173.
(2) Miyata, S. *Clays Clay Mater.* **1975**, *23*, 369.
(3) Tayler, R. M. *Clay Miner.* **1984**, *19*, 591.
(4) Drits, V. A.; Sokolova, T. N.; Sokolova, G. V.; Cherkashin, V. I. *Clays Clay Miner.* **1987**, *35*, 401.
(5) Fornasari, G.; Trifiro, F.; Vaccani, A.; Prinetto, F.; Ghiotti, G.; Centi, G. *Catal. Today* **2002**, *75*, 421.
(6) Basile, F.; Basini, L.; Fornasari, G.; Gazzano, M.; Trifiro, F.; Vaccari, A. *Chem. Commun.* **1996**, 2435.
(7) Basile, F.; Fornasari, G.; Gazzano, M.; Vaccari, A. *Appl. Clay Sci.* **2000**, *16*, 185.
(8) Brindly, G. W.; Kikkawa, S. *Clays Clay Miner.* **1980**, *28*, 87.
(9) Bellotto, M.; Rebours, B.; Clause, O.; Lynch, J.; Bazin, B.; Elkaim, E. *J. Phys. Chem.* **1996**, *100*, 8535.
(10) Pesic, L.; Salipurovic, S.; Markovic, V.; Vucelic, D.; Kagunya, W.; Jones, W. *J. Mater. Chem.* **1992**, *2*, 1069.
(11) Tsuji, M.; Mao, G.; Yoshida, T.; Tamaura, Y. *J. Mater. Res.* **1993**, *8*, 1137.
(12) Xu, Z. P.; Zeng, H. C. *Chem. Mater.* **2001**, *13*, 4564.

10.1021/cm051087w CCC: $30.25
Published on Web 08/24/2005

Table 1. Chemical Composition of HT and Pt−HT (2Pt/Al=0.03)

	mol mol^{-1}					
	Mg	Al	NO_3	H_2O	Pt	Cl
HT	0.74	0.26	0.26	0.36		
Pt−HT	0.74	0.26	0.26	0.36	0.004	0.015

of H_2.[13,14] The reduction of interlayer nitrate in the presence of Pt began at a low temperature (ca. 200 °C), where the surface area increased steeply up to ≥200 m^2 g^{-1}. To the best of our knowledge, this is the transformation of HT to a large surface area solid at lowest possible temperatures. It is suspected that exchanged Pt species play a role of catalyst to promote the thermal decomposition. Conventionally, the noble metals are introduced by coprecipitation to form mixed HT precipitates, or by incipient wet impregnation onto calcined HT.[1] The anion exchange and subsequent thermal decomposition are an interesting alternative method[13−15] because it is easy to synthesize highly dispersed noble metal catalysts supported on a wide variety of mixed oxides, which can be obtained from HT-like double hydroxides.

In the present paper, we have studied the formation mechanism of porous structure from $PtCl_6^{2-}$-exchanged Mg−Al−NO_3. To gain a better understanding on the catalytic role of Pt species in the interlayer, ion exchange of $PtCl_6^{2-}$ and thermal decomposition have been analyzed in detail using XRD, TPR, XAFS, XRF, TEM, and N_2 adsorption measurement. In particular, the reaction pathway of interlayer nitrate is discussed in relation to the chemical state of Pt species deposited inside the interlayer space. On the basis of the present results, the catalytic conversion of hydrotalcite phases into porous textures can be proposed as a novel catalyst preparation method.

Experimental Section

Preparation. Hydrotalcite-like $Mg_{0.74}Al_{0.26}(OH)_2(NO_3)_{0.26}\cdot 0.36H_2O$ was synthesized by coprecipitation at room temperature.[13,14] An aqueous solution of $Mg(NO_3)_2$ and $Al(NO_3)_3$ was added dropwise to 100 mL of 0.5 M aqueous ammonia with vigorous stirring. The resulting precipitate was centrifuged and washed thoroughly with distilled deionized water, followed by a drying overnight in vacuo. The powder of as-prepared precipitates was then dispersed in an aqueous solution of K_2PtCl_6 in the range of molar ratios, 0.03 ≤ 2Pt/Al ≤ 1.0, at room temperature for 24 h. The resultant $PtCl_6^{-}$-exchanged phases were heated in a stream of H_2 or air at elevated temperatures (200−700 °C) for 2−24 h prior to characterization. The unexchanged phase and exchanged phase at 2Pt/Al = 0.03 are denoted as HT and Pt-HT, respectively. Table 1 compares the chemical composition of these two samples.

Characterization. Powder X-ray diffraction pattern was measured with a diffractometer (Rigaku Miltiflex, Cu Kα, 30 kV, 30 mA) equipped with a diffraction beam graphite monochromator. The chemical composition was determined by an energy-dispersive X-ray fluorescence spectrometer (Horiba MESA-500W, Rh anode, 15/50 kV, 500/240 μA). The thermal decomposition of pristine and exchanged HT was analyzed by temperature programmed reduction (TPR) in a conventional flow reactor connected to a volumetric vacuum system and to a differential evacuation system. After evacuation at room temperature, as-prepared HT and Pt−HT were heated in a flowing gas mixture of 10% H_2/He (20 cm^3/min) at a constant rate (10 °C/min). Gas mixtures left from the sample were analyzed by a quadrupole residual gas analyzer mass spectrometer (Anelva M-100). The dispersion of Pt was determined by H_2-O_2 titration, using the pulsed flow technique at room temperature. After the reduction treatment in a flow of 10% H_2 at 400 °C and subsequent evacuation, Pt−HT was placed in flowing Ar and He to conduct O_2 and H_2 injections into the stream alternately just before the catalyst bed, respectively. The titration was carried out first with O_2, then with H_2, and finally with O_2 again. The effluent H_2 and O_2 were detected by using a TCD cell to determine the amounts of H_2 and O_2 molecules adsorbed onto Pt. The number of Pt atoms exposed on the surface (n_{Pts}) was calculated on assuming the ratio, $n_{H2}/2n_{Pts}$, to be unity. The dispersion of Pt is defined as n_{Pts}/n_{Pt}, where n_{Pt} is the number of total Pt atoms impregnated.

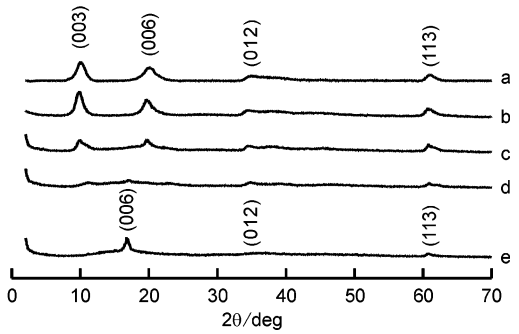

Figure 1. XRD patterns of as-prepared Pt−HT with different degrees of exchange: (a) 2Pt/Al = 0, (b) 0.03, (c) 0.15, (d) 0.30, and (e) 1.0.

The microstructure of as-decomposed solids was observed by TEM (JEOL 2000FX, 200 kV). The nitrogen adsorption and desorption isotherms at 77 K were measured using a Belsorp Mini instrument. The specific surface area was determined using the BET method. Total pore volume was calculated from N_2 adsorption at $p/p_0 = 0.99$. The pore size distribution curves were calculated using the Dollimine and Heal method[16] on the desorption branch.

The chemical environment of Pt in HT was studied by X-ray absorption fine structure (XAFS), which was performed on the BL-10B of Photon Factory, High Energy Accelerator Research Organization at Tsukuba (Proposal #2004G088) using a Si(311) channel-cut monochromator. Injection beam energy was 2.5 GeV and ring current was 300−450 mA. Pt L_{III}-edge spectra were recorded at room temperature in a transmission mode using the ionization chambers filled with the detector gases of 85% N_2 balanced with Ar for the incident beam and of Ar for the transmitted beam, respectively. A sample was pressed into a disk after its volume was adjusted by polyethylene powder to give appropriate absorbance at the edge energy for the XAFS measurement. After drying under reduced pressure overnight, the disk was packed into a polyethylene package under Ar atmosphere. The XAFS data were processed by a REX 2000 program (Rigaku). The EXAFS oscillation was extracted by fitting a cubic spline function through the postedge region. To extract the amplitude and phase shift function for Pt−Cl and Pt−O bonds, K_2PtCl_6 and PtO_2 were used as references.

Results

Figure 1 shows the XRD patterns of the as-prepared and $PtCl_6^{2-}$-exchanged HT with various degrees of exchange, 2Pt/Al. The pristine HT exhibited peaks indexed as the (003), (006), (012), and (113) reflections, which are attributed to

(13) Machida, M.; Hamada, S. *Chem. Commun*. **2003**, 1962.
(14) Hamada, S.; Machida, M. *Solid State Ionics*. **2004**, 81.
(15) Li, S.-P.; Xu, J.-J.; Chen, H.-Y. *Mater. Lett*. **2005**, *59*, 2090.
(16) (a) Dollimore, D.; Heal, G. R. *J. Appl. Chem*. **1964**, *14*, 109. (b) Dollimore, D.; Heal, G. R. *J. Colloid Interface Sci*. **1973**, *33*, 233.

Table 2. Interlayer Distance and Surface Area of Pt−HT and HT after Heating

sample	heating	interlayer distance (nm)	surface area ($m^2\ g^{-1}$)
Pt−HT	as prepared	0.88	
	200 °C, H_2	0.76	11
	300 °C, H_2	0.68	193
	400 °C, H_2		210
	500 °C, H_2		202
	600 °C, H_2		228
Pt−HT	200 °C, air	0.87	≤1
	300 °C, air	0.87	5
	400 °C, air		82
	500 °C, air		119
	600 °C, air		136
HT	as prepared	0.89	
	200 °C, H_2	0.88	≤1
	300 °C, H_2	0.88	5
	400 °C, H_2		82
	500 °C, H_2		119
	600 °C, H_2		136
HT	200 °C, air	0.89	≤1
	300 °C, air	0.87	≤1
	400 °C, air		80
	500 °C, air		107
	600 °C, air		112

the trigonal unit cell. From the d_{003} value, 0.89 nm, and the thickness of a brucite layer, 0.48 nm,[17,18] a gallery height of the as-prepared HT is estimated to be 0.41 nm. After 3% exchange by $PtCl_6^{2-}$ (2Pt/Al = 0.03), the diffraction pattern remained almost the same. Further exchange more than 15%, however, led to the shift of the (00*l*) reflections to lower 2θ and the simultaneous disappearance of the (003) peak owing to the change of the space group from *R*-3*m* (166) to *R*-3*c* (167). The (006) reflection remaining after the disappearance of the (003) peak implies that the interlayer distance increased from 0.89 to 1.04 nm because the gallery height was extended from 0.41 to 0.56 nm. The change is rationalized by the intercalation of $PtCl_6^{2-}$ with a diameter of ca. 0.53 nm[19] into each of the interlayers. Considering the positive charge on the brucite sheet, $PtCl_6^{2-}$ should also adsorb on the external surface of HT. However, these XRD results demonstrated that the Pt complex is present inside the interlayer space at any degree of exchange. A following study employed Pt−HT with 3% exchange (2Pt/Al = 0.03) for the characterization of thermal decomposition behavior.

Table 2 summarizes the interlayer distance of pristine HT and Pt−HT after heating in the stream of H_2 or air. It is worth noting that the interlayer distance, d_{003}, of Pt−HT after heating in H_2 decreased from 0.88 (as-prepared) to 0.68 nm (300 °C), whereas those of Pt−HT heated in air remained almost the same (0.88−0.87 nm). The pristine HT heated in air or H_2 also showed negligible change of interlayer distance (0.89−0.87 nm). It was reported that the contraction of interlayer distance is accompanied by the dehydration of carbonate-type HT, e.g., $Mg_{0.64}Al_{0.36}(OH)_2(CO_3)_{0.18}\cdot 0.46H_2O$.[8] But this is not the case for the present nitrate-type HT because the decreased interlayer distance could not be observed except for Pt−HT after heating in a flow of H_2.

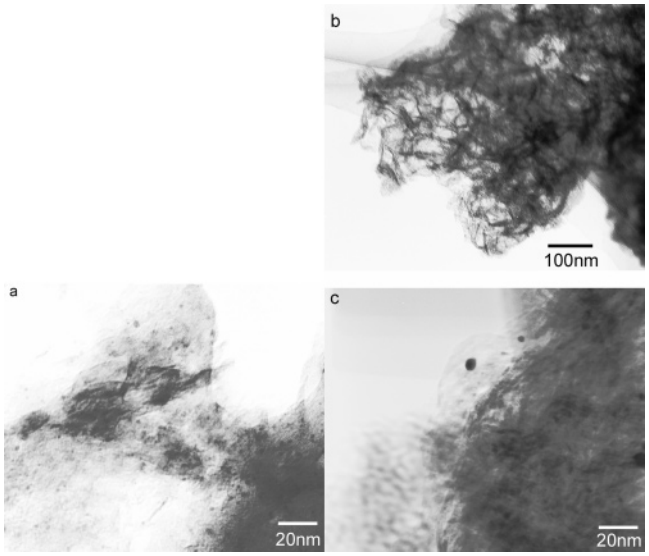

Figure 2. TEM photographs of Pt−HT after heating at (a) 300 °C and (b,c) 600 °C in H_2 (2Pt/Al = 0.03).

The different behavior between nitrate- and carbonate-types HTs should be associated with the interlayer configuration of each anion; e.g., in contrast to planar carbonates (CO_3^{2-}) lying as a monolayer parallel to the brucite layers, planar nitrates (NO_3^-) are tilt-lying or lying as double layer in the interlayer gallery.[18] Release of water molecules from the carbonate-type HT should therefore decrease the gallery height, whereas that of nitrate-type HT would be kept constant because NO_3^- anions play the role as pillars. With these facts taken into consideration, the decreased d_{003} of Pt−HT heated in H_2 should result from the removal of NO_3^-. Above 400 °C, the HT phase of both samples disappeared and yielded a rock-salt-like phase with a very low crystallinity. The amorphous nature of the product may be explained by assuming that heterogeneous shrinkage of the pillars (NO_3^- and $PtCl_6^{2-}$) at higher temperatures may destroy Bragg reflections.

Table 2 also shows the BET surface area of each sample. Before calcination, both HT and Pt−HT were nonporous solids with low surface areas ($<10\ m^2\ g^{-1}$). The surface area after heating was strongly influenced by the anion exchange and the heating atmosphere. Although the Pt−HT exhibited a considerable increase of surface area after heating in H_2 at as low as ≥200 °C, a nonporous product was preserved up to 400 °C after heating in air. On the other hand, the pristine HT was totally collapsed into a porous structure at ≥400 °C regardless of the heating atmosphere. It should therefore be noted that the increase of surface area occurred without destroying the layered structure only when the Pt−HT was heated in the presence of H_2. The surface area of Pt−HT after heating in H_2 was larger than $200\ m^2\ g^{-1}$, whereas other samples in Table 2 show the surface area smaller than $120\ m^2\ g^{-1}$.

Heating Pt−HT in H_2 at ≥100 °C caused a drastic color change from pale yellow to gray probably due to the deposition of metallic Pt in the interlayer. Figure 2 displays the TEM photograph of Pt−HT after heating in H_2 at different temperatures. The image of Pt−HT heated at 300 °C was taken with an incident beam perpendicular to the

(17) Bellotto, M.; Rebours, B.; Clause, O.; Lynch, J.; Bazin, B.; Elkaim, E. *J. Phys. Chem.* **1996**, *100*, 8527.
(18) Xu, Z. P.; Zeng, H. C. *J. Phys. Chem. B* **2001**, *105*, 1743.
(19) Restori, R.; Schwarzenbach, D. *Acta Crystallogr. A* **1996**, *52*, 369.

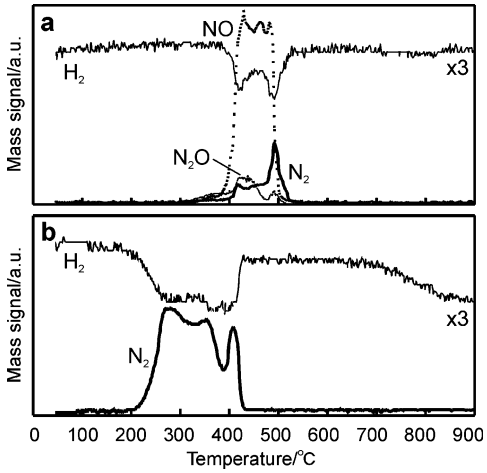

Figure 3. H_2-TPR profiles of (a) pristine HT and (b) Pt−HT (2Pt/Al = 0.03) measured in a stream of 10% H_2 balances with He. Heating rate: 10 °C min^{-1}.

basal plane of HT (a). The product consisted of lamellar particles with the size around a hundred nanometers. The surface of lamellar HT appears to be smooth and nonporous, but Pt particles smaller than 2 nm were already deposited. After heating at 600 °C, the lamellar HT phase was totally decomposed to form a three-dimensional porous texture (b). On the outer surface of the agglomerates, Pt grew into spherical particles of 2−5 nm in diameter (c). It should be noted that the contrast of Pt particles in (c) is much stronger than that in (a). This implies that Pt in (a) was embedded between brucite layers lying perpendicular to the incident beam.

These results suggest the occurrence of reactions between $PtCl_6^{2-}$, NO_3^-, and H_2 in the interlayer, which was next studied by TPR measurement. Figure 3 shows the gases left from HT or Pt−HT during heating in a 10% H_2/He flow at a constant rate of 10 °C min^{-1}. The H_2 consumption by pristine HT (a) presented two peak maxima at ca. 420 and 500 °C, where significant amounts of NO evolution occurred in coincident with total dehydroxylation due to the collapse of layered structure. However, the H_2 consumption by Pt−HT (b) began at much lower temperature of ca. 200 °C, where the gas product was not NO/NO_2 but largely composed of N_2. Judging from the absence of NO/NO_2 evolution as well as the completion of reduction at lower temperatures compared to the pristine HT, it is clearly demonstrated that Pt species catalyzed the reaction between H_2 and NO_3^- to evolve N_2. When the measurement was carried out in a flow of 5% O_2/He, both Pt−HT and HT yielded peaks of NO, NO_2, and O_2 at the same temperature of ca. 450 °C.

Figure 4 shows the dispersion of Pt measured by the H_2−O_2 titration at room temperature. The ratio of Pt atoms exposed on the surface to the total Pt (n_{Pts}/n_{Pt}) increased with a rise of heating temperature to give a constant value of ca. 0.6 above 500 °C. This corresponds to a Pt sphere with the diameter around 2 nm, which was observed in the TEM image (Figure 2c). According to Figure 2a, the deposition of Pt was also evident after heating at 300 °C. Nevertheless, very small n_{Pts}/n_{Pt} values observed at ≤400 °C are not consistent with the TPR profiles (Figure 3) and the large BET surface area of ca. 200 m^2 g^{-1} (Table 2). One plausible

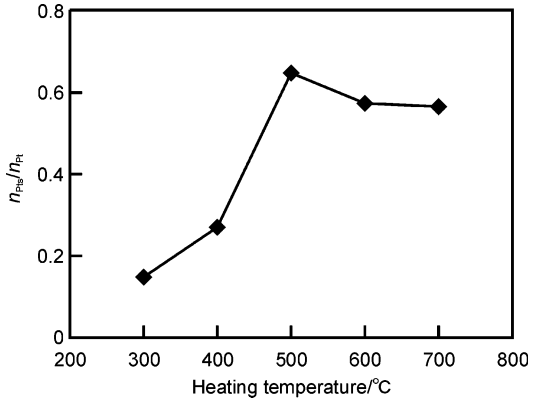

Figure 4. Dispersion (n_{Pts}/n_{Pt}) of Pt in Pt−HT (2Pt/Al = 0.03) after heating in H_2 at elevated temperatures.

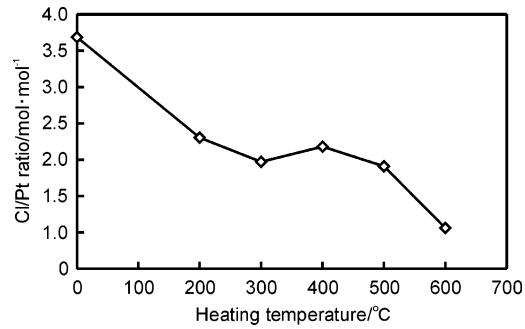

Figure 5. Amount of residual chloride in Pt−HT (2Pt/Al = 0.03) after heating in H_2 at elevated temperatures.

reason for such a low Pt dispersion is the morphology of Pt−HT formed at low temperatures. Because thin Pt particles were embedded in the interlayer (Figure 2a), their close contact would not allow gaseous H_2/O_2 to diffuse into the boundary and adsorb hereon. After the collapse of layered structure, a large part of Pt deposits would be exposed to the gas phase, so their size can be estimated by the H_2−O_2 titration.

Figure 5 exhibits the Cl/Pt ratio of Pt−HT after heating in H_2. Because the as-prepared $PtCl_6$-exchanged HT showed Cl/Pt = 3.7, the part of six chloride ligands of the Pt complex would already be lost in the ion-exchange process. The ratio decreased monotonically with an increase of heating temperatures, but the Cl/Pt ratio is still larger than unity even after heating at 600 °C, where the reduction by H_2 should be completed as was evident from Figure 3b. This means that the chloride species is difficult to be eliminated by the simple reduction in a H_2 flow.

The electronic structure and local environment of Pt species exchanged in the interlayer were studied by XAFS. Figure 6 shows Fourier transform of k^3-weighted Pt L_{III}-edge EXAFS for as-prepared Pt−HT and K_2PtCl_6. The structural parameters were obtained from the curve-fitting of the FT data. In the K_2PtCl_6 (a), a sole peak assigned to equivalent six Pt−Cl bonds appeared at a bond distance of 0.23 nm. The $PtCl_6$-exchanged HT before heating exhibited a very different result (b). The decreased intensity of the Pt−Cl peak suggests the coordination number decreasing from 6 to 3.2, which is close to the Cl/ Pt ratio (3.7) in Figure 5. In addition, another peak appeared at 0.20 nm is ascribable to a Pt−O bond with the coordination number of 2.9, but a second shell

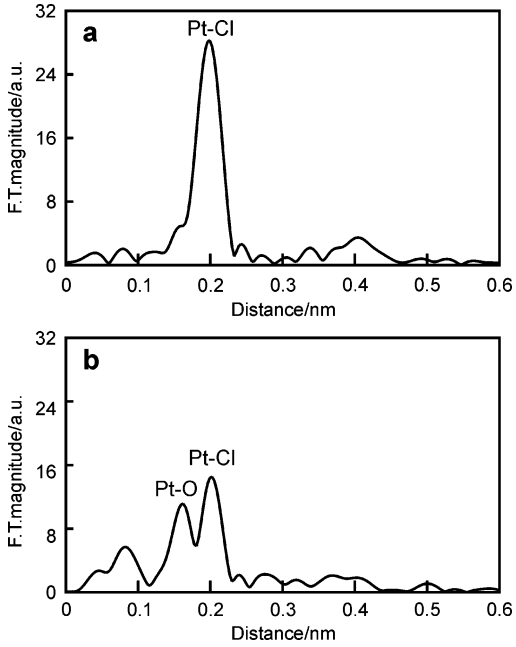

Figure 6. Fourier transforms of k^3-weighted Pt-L_{III} edge EXAFS of (a) K_2PtCl_6 and (b) Pt−HT (2Pt/Al = 0.03) before heating.

peak assigned to a Pt−O−Pt bond was not observed. These results indicate that the exchanged complex is not a bridge type with a Pt−O−Pt bond but a simple mononuclear type, which is coordinated by NO_3^- and Cl^- in the interlayer. The curve-fitting results for the first shell of EXAFS indicated that Pt species for as-prepared Pt−HT consisted of 3-fold coordinated Cl^- and 3-fold coordinated NO_3^-. After heating at 300 °C in H_2, the intensity of the Pt L_{III} white line was considerably decreased and the peak position was shifted to lower energy, indicating the reduction of Pt^{4+} to Pt^0. However, the coordination ascribable to a Pt−Cl bond was still observed in addition to Pt−Pt and Pt−O bonds. The calculated coordination numbers were very low, probably because various different Pt species were formed depending on the residual Cl^- concentration. In such a case, it is difficult to estimate the coordination number of Pt−Pt shell by the curve-fitting of FT-EXAFS oscillation. The detailed result of XAFS analysis of Pt−HT after heating will be presented in the forthcoming report.

The N_2 adsorption/desorption isotherms of HT and Pt−HT after heating in H_2 are compared in Figure 7. As is evident from Table 2, the thermal decomposition of pristine HT to form a large surface area solid was completed at 500 °C. The adsorption isotherm of the thus obtained solid was very similar to type IV defined in the IUPAC classification with a type H1 or H2 hysteresis loop, suggesting cylindrical pores. The increase of significant N_2 adsorption at p/p_0 = 0.6−0.8 supports the formation of mesopores. Quite different characteristics were observed for Pt−HT, which preserved a type H4 hysteresis typical for slit-shaped pores up to 500 °C. It is noteworthy that such two-dimensional pore structure was thermostable only when the Pt−HT was heated in H_2. Table 3 shows the total pore volumes of HT and Pt−HT after heating in H_2, which were calculated from the N_2 adsorption volume at p/p_0 = 0.99. Clearly, Pt−HT characterized by slit-shaped pores possessed pore volumes smaller than pristine HT consisting of cylindrical pores. Also, the

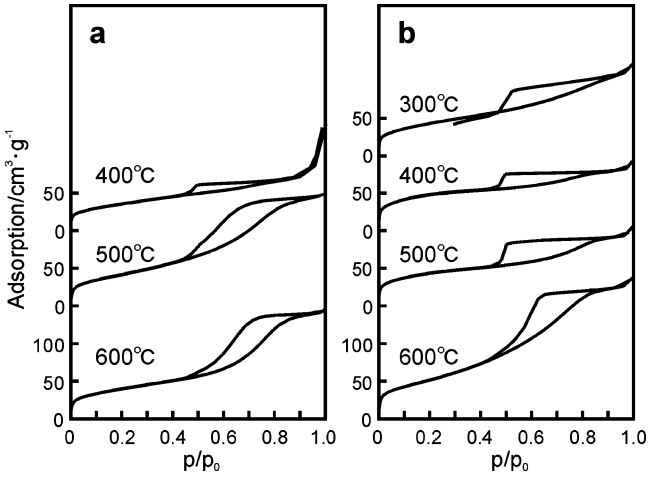

Figure 7. N_2 adsorption/desorption isotherms of (a) pristine HT and (b) Pt−HT (2Pt/Al = 0.03) after heating in H_2 at elevated temperature.

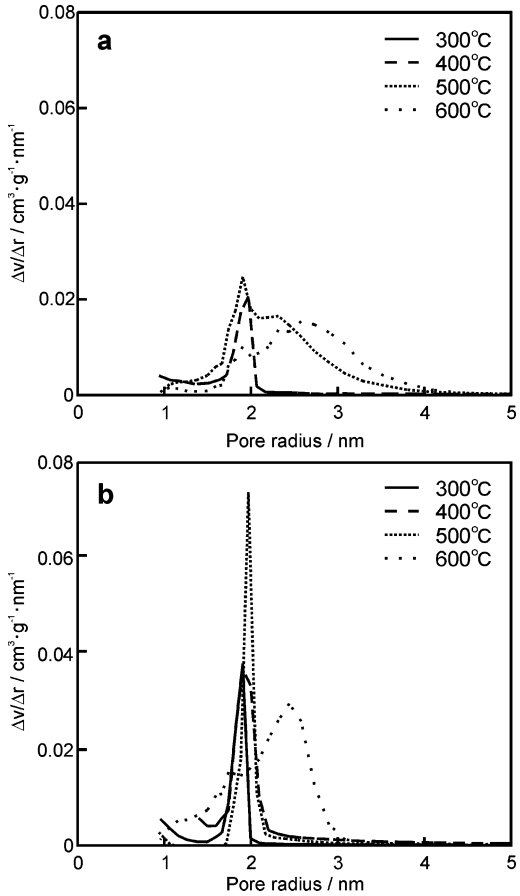

Figure 8. DH pore size distribution of (a) pristine HT and (b) Pt−HT (2Pt/Al = 0.03) after heating in H_2 at elevated temperatures.

Table 3. Total Pore Volumes (cm^3/g) of Pristine HT and Pt−HT after Heating at Different Temperatures

	heating temperature/°C			
	300	400	500	600
HT		0.22	0.23	0.23
Pt−HT	0.19	0.14	0.17	0.29

sudden increase of Pt−HT pore volume occurred when the slit-shaped pore was transformed into the cylindrical pore at 600 °C. The pore size distributions in the mesopore region were calculated from desorption isotherms by the DH method (Figure 8). The pristine HT after heating at 400 °C gave a

sole peak centered at 1.9 nm but further heating at higher temperatures increased the pore size and broadened the distribution. A similar change of the pore size distribution could be observed for the Pt−HT, but very sharp and intense distribution peaks after heating clearly suggested more uniform slit-shaped pores.

Discussion

It is well-known that the large specific surface area can be obtained upon thermal decomposition of HT irrespective of surface area of starting materials.[20,21] However, structural aspects of the decomposition process have not been understood before extensive studies carried out by Bellotto et al.[8] and Zeng and his co-worker.[12] They have reported that decomposition takes place in two steps: the dehydration of interlayer at ≤200 °C and subsequent collapse of layered structure in the range 300−400 °C. The first step is accompanied by a significant rearrangement of the octahedral brucite layer, where trivalent cations (Al^{3+}) migrate out of the layer to tetrahedral sites in the interlayer.[8] This step is not associated with a steep increase of surface areas. The second step consists of the decomposition of interlayer anions and the dehydroxylation of brucite layers, which cause the contraction of the hydroxide sheet to generate strains. Such strains would finally yield cratered surface texture,[22] which has frequently been observed for the thermally decomposed HT (Figure 2). This model can explain the reason why the sudden increase of surface area occurs when the layered structure of HT collapsed.

Interestingly, the present Pt−HT heated in H_2 is not such a case. The most important difference is that the interlayer NO_3^- is removed by the reaction with molecular H_2 before the dehydroxylation of brucite layers. As a result, the Pt−HT is converted into a porous texture without destroying a layered structure. One may point out that the reduction of NO_3^- in the Pt−HT would start even at 200 °C, but the increase of surface area requires the heating above 300 °C (Table 2). This disagreement is ascribable to a very low rate of reduction of NO_3^- at 200 °C because a strong Pt−Cl bond would inhibit the reduction to Pt metal as is evident from Figure 5. When we used a nitro complex, $Pt(NO_2)_4^{2-}$, in place of $PtCl_6^{2-}$, the reduction by H_2 took place much more smoothly, so the surface area increased from ≤1 to ca. 40 $m^2\ g^{-1}$ even after heating at 200 °C. With progress of the removal of NO_3^-, the nonporous interlayer is gradually converted into slit-shaped open gaps accessible by gaseous species. This mechanism is supported by the following facts: (i) the (00*l*) reflection in the XRD pattern remained after completion of NO_3^- removal and (ii) the N_2 adsorption isotherm indicated the presence of slit-shaped pores (Figure 7). Above 500 °C where total dehydroxylation of brucite layers occurs, this type of two-dimensional porous texture is finally transformed into a three-dimensional porous structure. Thus, the present study clearly demonstrates that the decomposition pathway of Pt−HT is quite different from that of unexchanged HT.

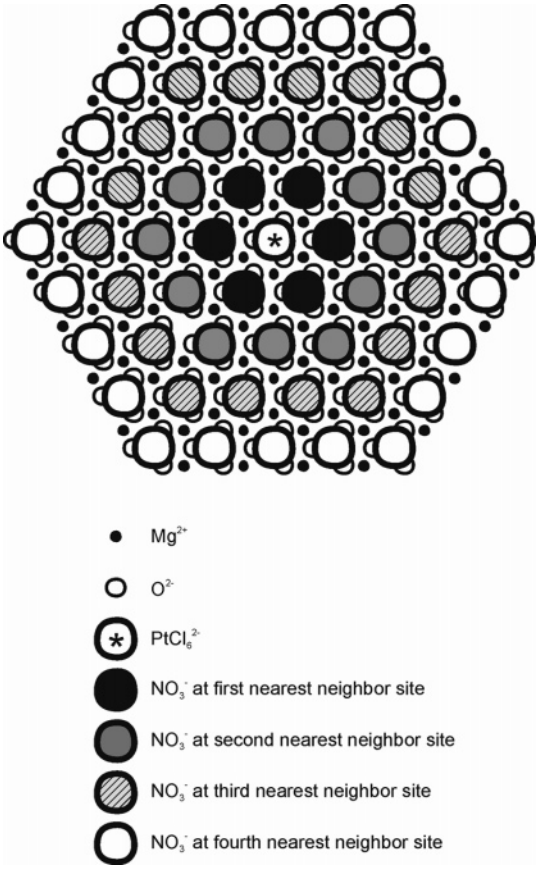

Figure 9. Schematic illustration of arrangement of NO_3^- around Pt complex in the interlayer of Pt−HT (2Pt/Al = 0.03).

One may guess that this phenomenon is a characteristic of nitrate-type phase because NO_3^- is easily reduced by H_2 to N_2 in the presence of noble metal catalysts such as Pt. However, the catalytic conversion inside such a two-dimensional narrow space is not well-known. Here, the catalytic role of Pt species in the interlayer should be discussed to prove the above pore-formation mechanism. As the XRF and XAFS results (Figures 5 and 6) indicate, the $PtCl_6^{2-}$ complexes accommodated in the interlayer are partly coordinated by NO_3^- in place of initial Cl^- ligands. Because the Pt complex can activate molecular hydrogen, the NO_3^- ligand thus formed near the edge of lamellar HT particles should first be removed by reaction with hydrogen to form N_2. This would yield a vacant site on the reduced $PtCl_x$ species, which can be subsequently occupied by NO_3^- ions lying in the interior. Such coordination/reduction cycles in the interlayer should substantially accelerate the removal of NO_3^- because of the increasing open space accessible by H_2 molecules.

Figure 9 shows the schematic illustration of the ideal arrangement of NO_3^- in the interlayer. Because two NO_3^- ions are replaced by one Pt complex, 3% exchange in the present system corresponds to the ratio of $NO_3^-/Pt = 65$. This is close to the model of Figure 9, where each Pt complex is surrounded by NO_3^- in the four neighboring layers ($NO_3^-/Pt = 60$). As shown in the TPR results (Figure 3b), the

(20) Clause, O.; Gazzano, M.; Trifiro, F.; Vaccari, A.; Zatorski, L. *Appl. Catal.* **1991**, *73*, 217.
(21) Clause, O.; Gazzano, M.; Coelho, M.; Zatorski, L. *Appl. Clays Sci.* **1993**, *8*, 169.
(22) Reichle, W. T.; Kang, S. Y.; Everhardt, D. S. *J. Catal.* **1986**, *101*, 352.

profiles of both N_2 and H_2 presented several overlapped peaks, suggesting the reduction process in consecutive stages. This means that, after the NO_3^- ligands are reduced at the lowest temperature of ca. 200 °C, the reduction would spread from the first to fourth nearest neighbors with an increase of temperatures. The observed N_2 evolution curves in Figure 3 can be decomposed into three peaks in the range of 200−450 °C, and first and second peaks at ≤390 °C correspond approximately to the number of NO_3^- within the third nearest neighbor layer. The third peak at ≥400 °C may originate from NO*x* evolved at the collapse of the layered structure because it overlaps with the evolution of NO from the pristine HT (Figure 2a). Actually, however, the reduction is more complicated due to the occurrence of the hydrogen spillover and coalescence of reduced Pt atoms to form Pt crystallites. In particular, hydrogen spillover cannot be excluded in the present reduction process of Pt−HT.

Conclusions

The following conclusions have emerged from the present study on the catalytic role of intercalated $PtCl_6^{2-}$ complex on the thermal decomposition of hydrotalcite-like Mg−Al−NO_3 materials.

(1) The catalytic role of Pt species is to accelerate the reaction between NO_3^- and H_2 in the interlayer to yield N_2. The reaction can accelerate the removal of interlayer NO_3^- before the collapse of layered structure to yield a slit-shaped pore structure. The pore structure is in complete contrast to the cylindrical pores observed for the pristine HT after thermal decomposition, which requires heating at ≥400 °C.

(2) Part of Cl^- ligands bound to Pt was substituted by NO_3^- lying in the interlayer. The nitrate ligand is then quickly reduced by activated hydrogen to N_2 to form a vacant site, which can subsequently be occupied by other nitrates. Such a coordination/reduction cycle is a possible reason why the interlayer nitrate anions are removed at low temperatures of ≥200 °C.

(3) At the initial stage of the reduction, Pt appears to grow as two-dimensional deposits in the interlayer of HT, but they were agglomerated to form spherical particles after the layered structure collapsed. The chloride species bound to Pt are difficult to remove completely. As an alternative complex, tetranitroplatinate, $Pt(NO_2)_4^{2-}$, would enable the synthesis of porous Pt−HT composites at lower temperatures.

Acknowledgment. The present study was financially supported by Grant-in-aid for Scientific Research from the Ministry of Education, Science, Sports, and Culture, Steel Industry Foundation for the Advancement of Environmental Protection Technology, and Kurita Water and Environment Foundation.

CM051087W